Supporting Information for

Investigating and Biomimicking the Surface Wetting Behaviors of Ginkgo Leaf

Shuaijun Pan, Rui Guo, and Weijian Xu*

Dr. Shuaijun Pan

State Key Laboratory of Chemo/Biosensing and Chemometrics, Institute of Polymer Science and Engineering, College of Chemistry and Chemical Engineering, Hunan University, Changsha 410082, China. Email: shuaijunpan@gmail.com

Miss Rui Guo

State Key Laboratory of Chemo/Biosensing and Chemometrics, Institute of Polymer Science and Engineering, College of Chemistry and Chemical Engineering, Hunan University, Changsha 410082, China.

Patent Examination Cooperation Hubei Center of the Patent Office, State Intellectual Property Office, Wuhan 430070, China.

Email: ruierlisa@sina.com

Dr. Weijian Xu

Corresponding Author

State Key Laboratory of Chemo/Biosensing and Chemometrics, Institute of Polymer Science and Engineering, College of Chemistry and Chemical Engineering, Hunan University, Changsha 410082, China. Email: weijianxu59@gmail.com

Movie Captions

Movie S1. *Water droplets impact on the fresh ginkgo leaf.* The shady side perfectly repels the continuous impacting water droplets as water drop readily bounces off the surface. The sunny side of ginkgo leaf could repel only a few impacting droplets which could bounce off the surface but with an obvious retention. The sunny side could not hold the composite Cassie-Baxter interface after a few impact, that is, the air plastron forms at the interface beaks thus droplet adhesion appears at last. In the video, droplets were released from 1~2 cm above the surface. The leaf was naturally lying on the horizontal table. A tilt angle of ~10° was formed due to the natural state of the leaf.

Movie S2. *Stain removal on the fresh ginkgo leaf.* The preset red ink droplet is easily and completely removed from the shady side of the ginkgo leaf by a strip of filter paper. The sunny side is left with obvious residue and cannot be removed completely with cut filter paper. The adhesion force at the water-epidermis interface of sunny side is higher than that of shady side.

Movie S3. *Air plastron observation.* Shady side forms a bright stable air plastron in water and no stains are left when being lifted out. Sunny side also forms an air plastron but relatively unstable as obvious water residues are left on the surface after taken out of the solution.

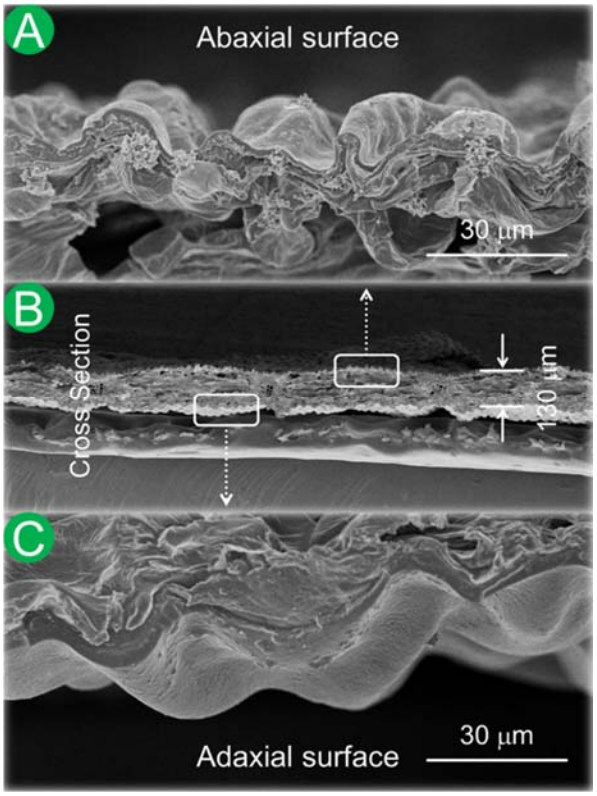

Figure S1. SEM images of dry ginkgo leaf. (A) Shady surface (abaxial surface). (B) Cross section. (C) Sunny surface (adaxial surface). Surface features collapse after drying.

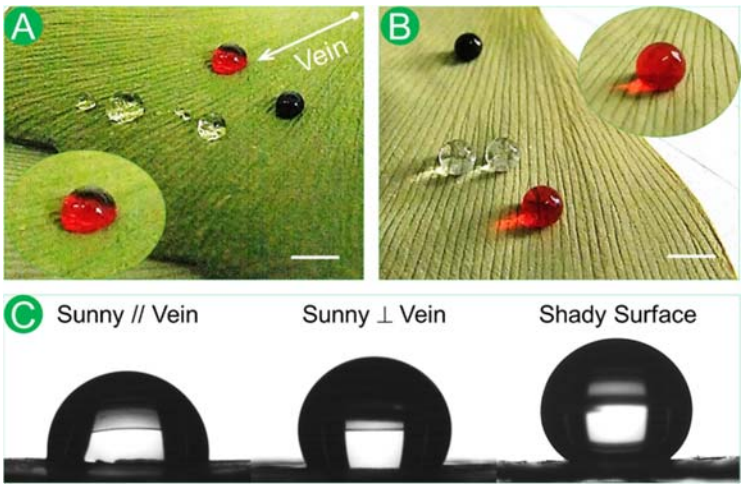

Figure S2. Wettability of dry ginkgo leaf. (A) Water drops stick on the dry sunny side with anisotropic wettability: water drop elongates along the vein. (B) Water drops ball up on the dry shady surface showing isotropic wettability. Scale bar is 5 mm. (C) Water silhouettes on the corresponding surface. Water contact angle on shady surface slightly decreases (~150º) due to the collapse of surface structure. Water contact angles on the sunny side decreases greatly while with a much smaller value (~90º) along the vein and a relatively larger value (~120º) perpendicular to the vein.

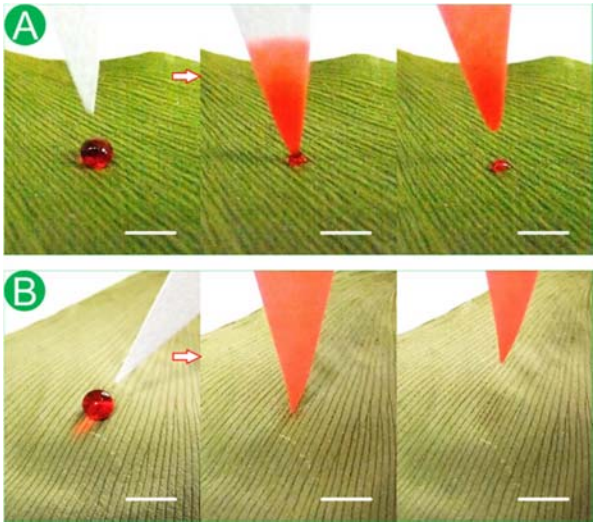

Figure S3. Stain removal of dry ginkgo leaf. (A) Sunny side. (B) Shady side. Shady side exhibits much more resistance to red ink, compared with sunny side which has a large contact angle hysteresis and red ink stain cannot be removed completely. Scale bar is 5 mm.

Table S1. Summary of equations for contact angle estimation.

Model	Cassie-Baxter Regime
Square packing spheres	$\cos\theta^* = -1 + \frac{1}{D^*}\left[\frac{\pi}{4}\left(1+\cos\theta_e\right)^2\right]$ $r_\phi = \frac{2\left(1+\cos\theta_e\right)}{\sin^2\theta_e} \qquad \phi_s = \frac{\pi\sin^2\theta_e}{4D^*}$ $f_{lv} = 1 - \frac{\pi\sin^2\theta_e}{4D^*} \qquad f_{sl} = \frac{\pi\left(1+\cos\theta_e\right)}{2D^*}$
Periodic cylindrical features[S1]	$\cos\theta^* = -1 + \frac{1}{D^*}\left[\sin\theta_e + \left(\pi-\theta_e\right)\cos\theta_e\right]$ $r_\phi = \frac{\pi-\theta_e}{\sin\theta_e} \qquad \phi_s = \frac{\sin\theta_e}{D^*}$ $f_{lv} = 1 - \frac{\sin\theta_e}{D^*} \qquad f_{sl} = \frac{\pi-\theta_e}{D^*}$

Note: $D^*_{particle} = \left(\frac{R+D}{R}\right)^2$ and $D^*_{fiber} = \frac{R+D}{R}$.

Table S2. Adaxial and abaxial surface properties of the fresh ginkgo leaf.

	Nomenclature	Adaxial Surface*	Abaxial Surface**
$2R$	Texture diameter	20 μm	20 μm
$2D$	Texture spacing	10 μm	10 μm
$2L$	Length of texture	60 μm	20 μm
λ	Aspect ratio	3	1
d^*	Linear spacing ratio of surface texture	1.5	1.5
D^*	Global spacing ratio of surface texture	2.25	1.5
H^*	Air thickness parameter	0.54	0.63
h_{air}	Calculated air thickness	10.9 μm	12.6 μm
ϕ_s	Area ratio of projected wet interface	0.64	0.33
r_ϕ	Surface roughness of wet area	1.36	1.59
f_{lv}	Fraction of liquid–air interface	0.36	0.67
f_{sl}	Fraction of solid–liquid interface	0.87	0.52

Note: Surface features are simplified as high aspect ratio ellipsoidal particles* and spherical particles**.

Table S3. Water contact angles and sliding angles on the natural and biomimetic surfaces.

Working Surfaces	Adv. CA	Rec. CA	Cal. ECA	As-placed CA	Sliding Angle
Flat wax coating	107	92	99	105	25
Fresh sunny side	146	130	136	136/126*	10/9.3*
Fresh shady side	157	154	155	156/144*	1/0.7*
Dry sunny side ⊥ vein	137	115	123	120	28
Dry sunny side // vein	99	85	92	90	20
Dry shady side	154	148	151	150	2
Flat PVA film	28	0	7	22	–
PVA replica of sunny side (negative)	11	0	3	8	–
PVA replica of shady side (negative)	9	0	3	5	–
Flat PS Film	107	85	95	104	27
PS replica of sunny side (positive)	143	126	133	130/125*	13/12.2*
PS replica of shady side (positive)	155	147	150	151/143*	3/2.4*

Note: * These values are in the set of measured/predicted. As-placed or static contact angles were predicted using the rewritten Cassie-Baxter equations (*e.g.* models of square packing particles and periodic fibers) derived in this work. For the CA calculation of shady surfaces, Equation S6 was applied, and Equation S12 was used for the sunny surfaces (see the supporting information Section S1). Sliding angles were predicted using the Furmidge method reported in the literatures.[S2-S6] Cal. ECA in the 4th column stands for the calculated equilibrium contact angle adopting Tadmor method.[S17] Sliding angle is discussed in detail in the supporting information Section S3. Unit of above values is degree (°). Derivation for contact angle is averaged within ±2° and sliding angle ±0.5°. ~10 μL water droplet was applied for the measurements. It is worth noting that the contact angles of flat polystyrene (PS) coating reported here is slightly different with those in the literatures[S23, S24] and we assume that the different nanoscale roughness introduced inevitably during the fabrication process (*i.e.* technical errors arising from dip-coating, evaporation, annealing, et al.) does matter the accuracy of the measurement.[S24-27]

Supplementary Discussions

Section S1. Contact Angle Estimation for Cassie-Baxter Regime

Particles constituting the practical surfaces can be simplified as spheres in theoretical calculations. Surfaces consisting of high aspect ratio features can be simplified as periodic alignments.

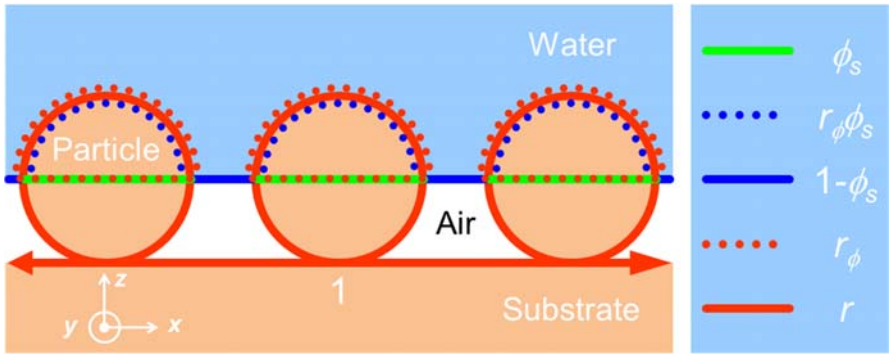

Figure S4. Schematic diagram of the cross section of spherical or fiber-like surfaces and characteristic geometrical parameters used in calculations.

To theoretically quantify the surface performance about wetting, parameters are defined above according to the literature.[S7-S8] ϕ_s is the area fraction of the air-liquid interface occluded by the surface texture (*i.e.* the ratio of the projected wet area to the total projected area). r_ϕ is the surface roughness of the wetted region (*i.e.* the ratio of the actual contacting surface to the projected wetted area). r is the global surface roughness (*i.e.* the ratio of the total surface area to the projected area). Thus, for a partially wetted surface ($\theta_e > 0^o$) shown above, the area fraction of liquid-solid interface is $f_{sl} = r_\phi \phi_s$ and that of liquid-air interface is $f_{lv} = 1 - \phi_s$.

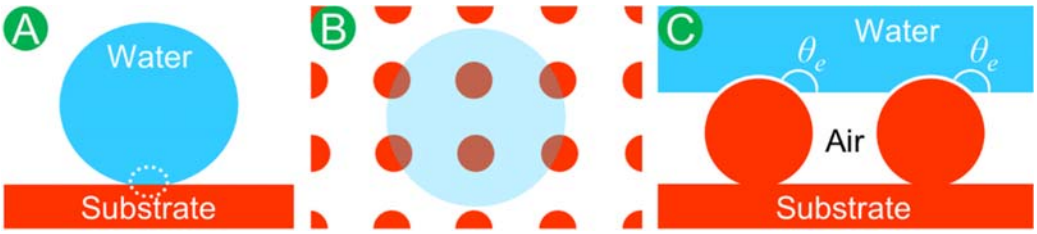

Figure S5. Schematic diagram shows side view (A) and top view (B) of a water drop ball-up the substrate in composite Cassie-Baxter state and the zoom-in interface (C) illustrating the local air-water-solid contact.

When a millimeter-sized water drop contacts with a non-wetting rough surface, provided the drop size is much greater than the surface feature size and the line tension applied on the triple line could be negligible, system free energy will reach global minimum as the apparent contact angle θ^* of the composite interface attains a value derived from the following Cassie-Baxter equations:[S9-S16]

$$\cos\theta^* = f_{sl}\cos\theta_e - f_{lv} \qquad \text{(S1)}$$

$$\cos\theta^* = r_\phi \phi_s \cos\theta_e + \phi_s - 1 \qquad \text{(S2)}$$

Effectively the above two equations are all referred as mixed wetting state – a droplet partially wets the surface and partially sits on air pockets, which is commonly used in solving wetting problem on rough porous surfaces especially those with curvatures like cylindrical fibers or particles[S21]. However, in solving the wetting problem of the most commonly considered surfaces in the literature as vertical arrays of flat-top pillars[S22], the original CB equation has been slightly transformed in a more coherent one ($f_{sl} + f_{lv} = 1$), a form which has also been referred as pure

Cassie state (especially holds for surfaces composed of flat-top pillars and holes). In our case, the spherical texture represents a re-entrant geometry – the solid-liquid area is function of liquid penetration depth. Thus, regarding the roughness of wetted area ($r_\phi \geq 1$), the sum of solid-liquid area (f_{sl}) and liquid-vapor area (f_{lv}) is always greater than 1.[S7, S9] Equation S2 is an extended form of the Cassie relation (a generalized textural wetting equation). Actually, the CB equation with a unit sum of coefficients (pure Cassie State) is just a specific form of Equation S2 if the roughness of wetted area (r_ϕ) is equal to 1 (*i.e.* flat-top pillars and holes referred previously).[S12] In order to better describe the mixed wetting state when water drops come to contact with the surface of ginkgo leaf, the above Cassie-Baxter equations could be rewritten as the following.

Case I. As for a partially wetted surface featured by ***square pitch arranged spheres***, we have:

$$r_\phi = \frac{\pi R^2\left(1+\cos\theta_e\right)}{\frac{1}{2}\pi\left(R\sin\theta_e\right)^2} = \frac{2\left(1+\cos\theta_e\right)}{\sin^2\theta_e} \qquad \text{(S3)}$$

$$\phi_s = \frac{\pi\left(R\sin\theta_e\right)^2}{\left(2R+2D\right)^2} = \frac{\pi\sin^2\theta_e}{4D^*} \qquad \text{(S4)}$$

Here D^* is the global spacing ratio of the surface texture, it is the square of the linear spacing ratio d^* for spherical features:

$$D^* = \left(\frac{R+D}{R}\right)^2 = d^{*2} \qquad \text{(S5)}$$

Thus, Cassie-Baxter equation can be transformed as:

$$\cos\theta^* = -1 + \frac{1}{D^*}\left[\frac{\pi}{4}\left(1+\cos\theta_e\right)^2\right] \qquad \text{(S6)}$$

And the area fraction of solid-liquid interface f_{sl} and liquid-air interface f_{lv} is computed as:

$$f_{sl} = \frac{\pi\left(1+\cos\theta_e\right)}{2D^*} \qquad \text{(S7)}$$

$$f_{lv} = 1 - \frac{\pi\sin^2\theta_e}{4D^*} \qquad \text{(S8)}$$

Case II. As for a partially wetted surface composed of ***periodic cylinders or high aspect ratio spheroids*** with $\lambda >> 1$, we have:[S1]

$$r_\phi = \frac{R\left(\pi-\theta_e\right)}{R\sin\theta_e} = \frac{\pi-\theta_e}{\sin\theta_e} \qquad \text{(S9)}$$

$$\phi_s = \frac{R\sin\theta_e}{R+D} = \frac{\sin\theta_e}{D^*} \qquad \text{(S10)}$$

Here, the global spacing ratio D^* is equal to the linear spacing ratio d^* for fiber features:

$$D^* = \frac{R+D}{R} = d^* \qquad \text{(S11)}$$

Thus, Cassie-Baxter equation and the interface fractions can be transformed as:

$$\cos\theta^* = -1 + \frac{1}{D^*}\left[\sin\theta_e + \left(\pi-\theta_e\right)\cos\theta_e\right] \qquad \text{(S12)}$$

$$f_{sl} = \frac{R\left(\pi-\theta_e\right)}{R+D} = \frac{\pi-\theta_e}{D^*} \qquad \text{(S13)}$$

$$f_{lv} = 1 - \frac{\sin\theta_e}{D^*} \qquad \text{(S14)}$$

Section S2. Thickness Estimation of Trapped Air Layer

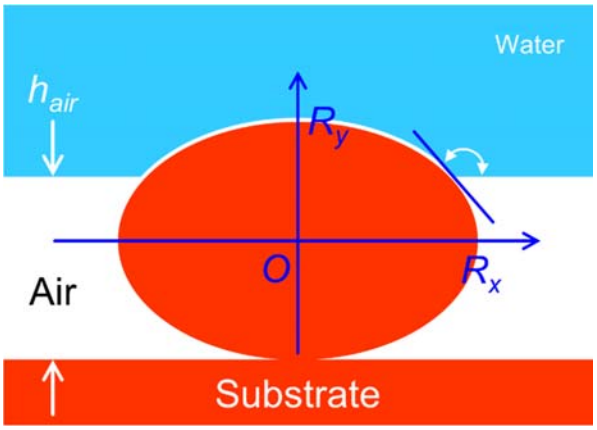

Figure S6. Rectangular coordinate system for the calculation of trapped air layer for non-embedded spheroidal particles (*i.e.* spherical or ellipsoidal features).

Build a two-dimensional rectangular coordinate system first, and then place the lying spheroid particle at the origin of coordinates. The cross-section of the particle appears as an ellipsoid. The intercepts are the particle radii along X axis (R_x) and Y axis (R_y) respectively. Then the elliptic equation is obtained:

$$\frac{x^2}{R_x^2}+\frac{y^2}{R_y^2}=1 \qquad \text{(S15)}$$

Consider the contacting water locally reaches the equilibrium Young's contact angle θ_e at point P (m, n) on the elliptic curve, the relation between m and n is:

$$\frac{m^2}{R_x^2}+\frac{n^2}{R_y^2}=1 \qquad \text{(S16)}$$

The tangent slope at point P is given by the derivative of the elliptic equation:

$$k = \frac{dy}{dx} = -\frac{R_y^2}{R_x^2}\frac{n}{m} \qquad \text{(S17)}$$

$$k = \tan\theta_e \qquad \text{(S18)}$$

By substituting Equation S16–18 into Equation S15, the coordinate of *P* along Y axis is obtained:

$$n = \pm \frac{R_y}{\sqrt{\left(\frac{R_x}{R_y}\tan\theta_e\right)^2 + 1}} \qquad \text{(S19)}$$

Then, the air thickness is given by:

$$h_{air} = R_y \pm \frac{R_y}{\sqrt{\left(\frac{R_x}{R_y}\tan\theta_e\right)^2 + 1}} \qquad \text{(S20)}$$

Here, plus sign applies for hydrophobic coating, that is, the equilibrium Young's contact angle $\theta_e \geq 90^\circ$, and minus for $\theta_e \leq 90^\circ$.

A dimensionless factor for the trapped air layer thickness is defined as:

$$H^* \equiv \frac{h_{air}}{2R_y} \qquad \text{(S21)}$$

And a diameter factor (aspect ratio) of the particle is defined as:

$$\lambda \equiv \frac{R_x}{R_y} \qquad \text{(S22)}$$

Then, a dimensionless form of Equation S20 is obtained by defining R_y as unit ($R_y \equiv 1$):

$$H^* \equiv \frac{h_{air}}{2R_y} = \frac{1}{2}\left[1 \pm \frac{1}{\sqrt{(\lambda \tan\theta_e)^2 + 1}}\right] \qquad \text{(S23)}$$

A final form is obtained by defining a reference thickness $H_{ref} \equiv 2R_y$:

$$H^* \equiv \frac{h_{air}}{H_{ref}} = \frac{1}{2}\left[1 \pm \frac{1}{\sqrt{(\lambda \tan\theta_e)^2 + 1}}\right] \qquad \text{(S24)}$$

Equation S24 provides a general estimation of air trapped at the air–liquid–solid interface for contacting surfaces with different features (λ) and Young's wettability (θ_e). By careful designing surface textures and controlling the surface wettability, extreme liquid resistance may be achieved in the development of functional surfaces (*i.e.* robust surface resisting impact of liquid such as the shady surface of a fresh ginkgo leaf), and it is worth note that not thick enough air plastron may cause the triple interface to break down (i.e. unstable plastron at the sunny side of ginkgo leaf which causes wetting transition after continuous water impact).

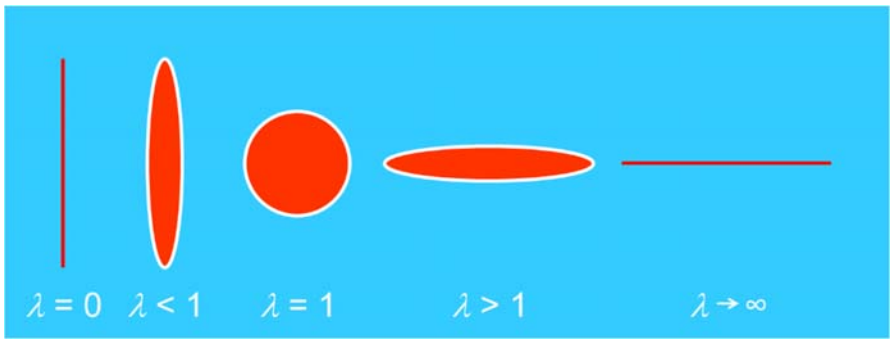

Figure S7. Different particle morphologies characterized by dimensionless aspect ratio λ .

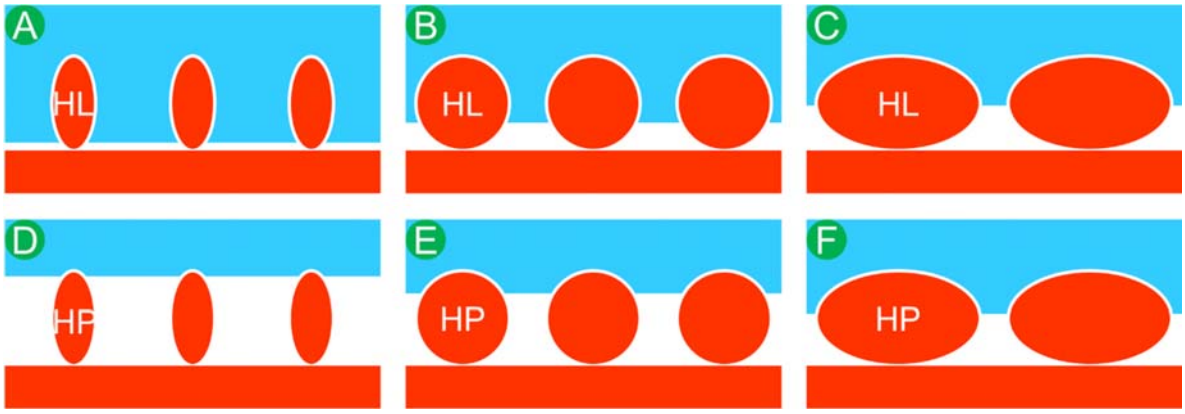

Figure S8. The effect of surface features (vertically equal) on the air plastron thickness at the triple contact region. Spheroid particles (λ>1) have different air thickness at spherical section (B, E) and ellipsoidal section (C, F). Least air thickness arises at ellipsoidal section for hydrophobic (θ_e > 90º) particles (F) and spherical section for hydrophilic (θ_e < 90º) particles (B). As for the trapped air thickness for ellipsoids (λ<1) (A, D) comparing with sphere (B, E), thinner air layer appears in ellipsoids for hydrophilic (θ_e < 90º) particles (A) and spheres for hydrophobic (θ_e > 90º) particles (E). The order of the above illustrated air thickness is D > E > F > C > B > A.

Section S3. Sliding Angle Calculations

Consider a liquid droplet on a tilted at an angle ω relative to the horizontal. By balancing the work done by droplet gravity and surface tension during wetting/dewetting, the tilt angle at which the drop starts to slide is given by the following relation[S2-S6]:

$$\sin\omega = \frac{2\gamma_{lv} D_{TCL}\left(\cos\theta^*_{rec} - \cos\theta^*_{adv}\right)}{\pi\rho g V} \qquad \text{(S25)}$$

Here, ρ and γ_{lv} are the density and surface tension of the liquid, respectively, g is the acceleration due to gravity, V is the volume of the droplet, and D_{TCL} is the averaged diameter of the triple phase contact line perpendicular to the sliding direction, which can be predicted using an average apparent contact angle $\overline{\theta}^*$. The width of the droplet can then be computed as:

$$D_{TCL} \approx 2\sin\overline{\theta}^* \sqrt[3]{\frac{3V}{\pi\left(2 - 3\cos\overline{\theta}^* + \cos^3\overline{\theta}^*\right)}} \qquad \text{(S26)}$$

$$\cos\overline{\theta}^* = \frac{\cos\theta^*_{rec} - \cos\theta^*_{adv}}{2} \qquad \text{(S27)}$$

Our experimentally measured sliding angles match reasonably well with those predicted by equations above (*see* Table S3).

Tadmor method[S17] may also be used in calculating the average contact angle (i.e. calculated equilibrium contact angle θ_E) thus further for the calculation of the sliding angle.

$$\theta_E = \arccos\left(\frac{r_A \cos\theta_A + r_R \cos\theta_A}{r_A + r_R}\right) \quad \text{(S28)}$$

$$r_A = \left(\frac{\sin^3\theta_A}{2 - 3\cos\theta_A + \cos^3\theta_A}\right)^{1/3} \quad \text{(S29)}$$

$$r_R = \left(\frac{\sin^3\theta_R}{2 - 3\cos\theta_R + \cos^3\theta_R}\right)^{1/3} \quad \text{(S30)}$$

Here θ_A is the advancing contact angle and θ_R is the receding contact angle. Although the Tadmor method is commonly used for flat surface, the calculated equilibrium contact angle (using the values obtained on our surfaces) matches well with the as-placed contact angle (see Table S3), since the value of as-placed contact angle falls between that of advancing and receding contact angles and at some point matches that of the equilibrium contact angle depending on the drop size.[S18]

Additionally, sliding angle is an expression of liquid retention on the surface – lateral (retention or adhesion) force applied on the surface plays an important role in the interaction of liquid with the solid surface. The related lateral forces may be calculated or experimentally measured adopting the approaches reported in the literatures.[S2, S5, S19-S20] By investigating the physical forces between a droplet and the contacting surface (*i.e.* tilt or horizontally placed), it may offer another way in revealing the distinct wetting behaviors of ginkgo leaf (see Movies S1-S3).

Supporting References

S1. Choi, W.; Tuteja, A.; Chhatre, S.; Mabry, J. M.; Cohen, R. E.; McKinley, G. H. Fabrics with Tunable Oleophobicity. *Adv. Mater.* **2009,** *21*, 2190-2195.

S2. Furmidge, C. G. L. Studies at Phase Interfaces I. The Sliding of Liquid Drops on Solid Surfaces and A Theory for Spray Retention. *J. Colloid Sci.* **1962,** *17*, 309-324.

S3. Choi, W.; Tuteja, A.; Mabry, J. M.; Cohen, R. E.; McKinley, G. H. A Modified Cassie-Baxter Relationship to Explain Contact Angle Hysteresis and Anisotropy on Non-wetting Textured Surfaces. *J. Colloid Interface Sci.* **2009,** *339*, 208-216.

S4. Kota, A. K.; Li, Y.; Mabry, J. M.; Tuteja, A. Hierarchically Structured Superoleophobic Surfaces with Ultralow Contact Angle Hysteresis. *Adv. Mater.* **2012,** *24*, 5838-5843.

S5. Dussan V., E. B. On the Ability of Drops or Bubbles to Stick to Non-horizontal Surfaces of Solids. Part 2. Small Drops or Bubbles Having Contact Angles of Arbitrary Size. *J. Fluid. Mech.* **1985,** *151*, 1-20.

S6. Dimitrakopoulos, P.; Higdon, J. J. L. On the Gravitational Displacement of Three-dimensional Fluid Droplets from Inclined Solid Surfaces. *J. Fluid. Mech.* **1999,** *395*, 181-209.

S7. Tuteja, A.; Choi, W.; Mabry, J. M.; McKinley, G. H.; Cohen, R. E. Robust Omniphobic Surfaces. *Proc. Natl. Acad. Sci. U. S. A.* **2008,** *105*, 18200-18205.

S8. Chhatre, S. S.; Choi, W.; Tuteja, A.; Park, K.-C. K.; Mabry, J. M.; McKinley, G. H.; Cohen, R. E. Scale Dependence of Omniphobic Mesh Surfaces. *Langmuir* **2010,** *26*, 4027-4035.

S9. Cassie, A. B. D.; Baxter, S. Wettability of Porous Surfaces. *Trans. Faraday Soc.* **1944,** *40*, 546-551.

S10. Cassie, A. B. D.; Baxter, S. Large Contact Angles of Plant and Animal Surfaces *Nature* **1945,** *155*, 21-22.

S11. Marmur, A.; Bittoun, E. When Wenzel and Cassie Are Right: Reconciling Local and Global Considerations. *Langmuir* **2009,** *25*, 1277-1281.

S12. Bormashenko, E. General Equation Describing Wetting of Rough Surfaces. *J Colloid Interface Sci.* **2011,** *360*, 317-319.

S13. Miwa, M.; Nakajima, A.; Fujishima, A.; Hashimoto, K.; Watanabe, T. Effects of the Surface Roughness on Sliding Angles of Water Droplets on Superhydrophobic Surfaces. *Langmuir* **2000,** *16*, 5754-5760.

S14. Wong, T. S.; Ho, C. M. Dependence of Macroscopic Wetting on Nanoscopic Surface Textures. *Langmuir* **2009,** *25*, 12851-12854.

S15. Marmur, A.; Krasovitski, B. Line Tension on Curved Surfaces: Liquid Drops on Solid Micro- and Nanospheres. *Langmuir* **2002,** *18*, 8919-8923.

S16. Marmur, A. Wetting on Hydrophobic Rough Surfaces: To be Heterogeneous or NOT to be? *Langmuir* **2003,** *19*, 8343-8348.

S17. Tadmor, R. Line Energy and the Relation between Advancing, Receding, and Young Contact Angles. *Langmuir* **2004**, *20*, 7659-7664.

S18. Tadmor, R.; Yadav, P. S. As-placed Contact Angles for Sessile Drops. *J Colloid Interface Sci.* **2008,** *317*, 241-246.

S19. Tadmor, R.; Bahadur, P.; Leh, A.; N'guessan, H. E.; Jaini, R.; Dang, L. Measurement of Lateral Adhesion Forces at the Interface between a Liquid Drop and a Substrate. *Phys. Rev. Lett.* **2009**, *103*, 266101.

S20. Yadav, P. S.; Bahadur, P.; Tadmor, R.; Chaurasia, K.; Leh, A. Drop Retention Force as a Function of Drop Size. *Langmuir* **2008**, *24*, 3181-3184.

S21. Bormashenko, E. Wetting Transitions on Biomimetic Surfaces. *Phil. Trans. R. Soc. A* **2010**, *368*, 4695-4711.

S22. Öner, D.; McCarthy, T. J. Ultrahydrophobic Surfaces. Effects of Topography Length Scales on Wettability. *Langmuir* **2000**, *16*, 7777-7782.

S23. Bormashenko, E.; Pogreb, R.; Stein, T.; Whyman, G.; Erlich, M.; Musin, A.; Machavariani, V.; Aurbach, D. Characterization of Rough Surfaces with Vibrated Drops. *Phys. Chem. Chem. Phys.* **2008**, *10*, 4056-4061.

S24. Zheng, J.; He, A.; Li, J.; Xu, J.; Han, C. C. Studies on the Controlled Morphology and Wettability of Polystyrene Surfaces by Electrospinning or Electrospraying. *Polymer* **2006**, *47*, 7095-7102

S25. Wang, R.; Cong, L.; Kido, M. Evaluation of the Wettability of Metal Surfaces by Micro-pure Water by Means of Atomic Force Microscopy. *Appl. Surf. Sci.* **2002**, *191*, 74-84.

S26. Bormashenko, E.; Bormashenko, Y.; Whyman, G.; Pogreb, R.; Musin, A.; Jager, R.; Barkay, Z. Contact Angle Hysteresis on Polymer Substrates Established with Various Experimental Techniques, Its Interpretation, and Quantitative Characterization. *Langmuir* **2008**, *24*, 4020-4025.

S27. Erbil, H. Y.; Demirel, A. L.; Avci, Y.; Mert, O. Transformation of a Simple Plastic into a Superhydrophobic Surface. *Science* **2003**, *299*, 1377-1380.